Recursive T-Matrix Methods for Scattering from Multiple Dielectric and Metallic Objects*

Adnan Şahin Eric L. Miller
Center for Electromagnetics Research,
235 Forsyth Building, 360 Huntington Ave.
Northeastern University, Boston, MA 02115
Telephone: (617) 373-8386
Telefax : (617) 373-8627
email: adnan@cdsp.neu.edu

February 14, 1997

Abstract

We present an efficient, stable, recursive T-matrix algorithm to calculate the scattered field from a heterogeneous collection of spatially separated objects. The algorithm is based on the use of higher order multipole expansions that are typically employed in recursive T-matrix techniques. The use of these expansions introduces instability in the recursions developed in [1, 3] specifically in the case of near field computations. By modifying the original recursive algorithm to avoid these instabilities we arrive at a flexible and efficient forward solver appropriate for a variety of scattering calculations. The algorithm can be applied when the objects are dielectric, metallic, or a mixture of both. We verify this method for cases where the scatterers are electrically small (fraction of λ) or relatively large (1-2 λ). While developed for near field calculation, this approach is applicable for far field problems as well. Finally, we demonstrate that the computational complexity of this approach compares favorably with comparable recursive algorithms.

Submitted to *IEEE Trans. on Antennas and Propagation* in February, 1997.

*This work was supported in part DOE contract DE-FC07-95ID13395, NSF Grant MIP-9623721, and by subcontract GC123920NDG from Boston University under the AFOSR MURI Program on Reduced Signature Target Recognition

1 Introduction

Calculation of scattered electromagnetic fields is of interest in many different science areas. For example, an important component of many ground penetrating radar (GPR) problems is the efficient computation of the scattered fields produced by a collection of buried objects when illuminated by a radar source. The choice of technique for computing these fields is often driven by a variety of factors including computational complexity and the flexibility to handle easily a wide range of configurations of scatterers. In applications such as mine detection and hazardous waste removal objects can be either dielectric, metallic or mixtures. Their sizes can range from sub-wavelength to a few multiples of a wavelength. Therefore, one desires an efficient, flexible forward solver that is useful both for analysis and that can be incorporated into signal processing algorithms.

The most popular forward solver for these and related complex scattering problems, the Method of Moments (MoM) [6], is based on a fine discretization of the region of interest and requires the inversion of a large dense matrix to calculate the scattered field. As this task requires $O(N^3)$ calculations where N is the number of grid points, MoM is known to be quite computationally intensive. While fast multipole techniques [9] are useful for reducing the complexity of MoM-type linear systems, these algorithms are typically used for metallic objects and have theoretical difficulties with the spurious modes that can be circumvented only by "complexification" [12]. Finite difference techniques are also frequently used as forward solvers and like MoM rely on a full space discretization. Although the resulting matrices are sparse, one still faces the delicate task of specifying an absorbing boundary condition to terminate the computational grid.

Here we consider the use of transition matrix (T-matrix) methods [14,15] for solving the scattering problems of interest. Unlike MoM and finite differences, the T-matrix approach does not require an absorbing boundary condition and substitutes the discretization of space with harmonic

expansions of the fields thereby reducing the number of unknowns for a wide range of problems. For scattering problems involving single objects, this technique is applicable for metallic and dielectric scatterers. For problems involving multiple objects, Chew and co-workers have pioneered the development of a number of fast, recursive T-matrix algorithms for determining the scattered fields in a variety of scenarios [1–4, 8, 13]. For example, in [3], problems involving electrically large dielectric objects are considered. By tesselating the objects into many small sub-scatterers and using low order multipole expansions of the fields for each sub-scatterer the authors arrive at a highly efficient, T-matrix based algorithm for computing the scattered fields. In [4], Chew et.al. consider a scattering problem involving a group of metallic strips. Here the method of moments is used to compute the T-matrices for each, individual strip and the same recursion as in [13] is employed to solve the overall, multi-object scattering problem.

The motivation for the algorithm developed in this paper is the need to solve scattering problems for the GPR-type geometry shown in Fig. 1. Specifically, we are interested in the development and verification of a recursive algorithm capable of computing scattered fields from multiple dielectric and/or metallic objects in the near field. For simplicity, we considered an E_z polarized planewave incident on a two dimensional problem geometry in which multiple scatterers each possessing a circular cross-section (i.e. infinite circular cylinders) are located in an infinite medium of constant, complex permittivity. Because the use of a tesselated scheme is inappropriate for metallic objects, to handle this mixed-object problem we formulate a recursive algorithm based on high order harmonic expansions for the full scatterers. We demonstrate that this approach causes instabilities in the original recursive algorithm when near field computations are required. By modifying these recursions we obtain a stable algorithm which avoids these instabilities and which is capable of accurate near and far field calculations for the mixed scatterer problem of interest. Finally, we

demonstrate that this approach retains the low computational complexity of the method in [3].

The remainder of this paper is organized as follows. In Section 2 we review the T-matrix theory for single scatterers and the recursive T-matrix algorithm for multiple scatterers. In Section 3, we discuss how T-matrix techniques can be applied to GPR geometries, and we will present two alternative approaches to calculate the scattered field and the modification in the recursive algorithm. In Section 4, we will discuss the results and show examples and finally in Section 5 we will draw conclusions and suggest future work.

2 T-Matrix Background

2.1 Single Scatterer T-matrix

The total scalar electromagnetic (or acoustic) wave in a homogeneous background with a homogeneous scatterer is given by[1]:

$$\psi(\underline{r}) = \psi^{inc}(\underline{r}) + \psi^{sca}(\underline{r}) \tag{1}$$

where $\psi^{inc}(\underline{r})$ is the wavefield incident on the scatterer and $\psi^{sca}(\underline{r})$ is the field scattered from the object.

Applying the Poincaré-Huygens principle and the Gauss theorem we can write the total field outside the scatterer as [11]:

$$\psi(\underline{r}) = \psi^{inc}(\underline{r}) + \int_S dS' \{\psi_+(\underline{r'})\nabla' g(k|\underline{r} - \underline{r'}|) - [\nabla'_+\psi(\underline{r'})]g(k|\underline{r} - \underline{r'}|)\} \tag{2}$$

where S is a piecewise smooth surface enclosing the scatterer, ψ_+ and $\nabla'_+\psi$ are the total field $\psi(\underline{r})$ and its gradient on the outer surface of the scatterer, and $g(k|\underline{r} - \underline{r'}|)$ is the free space Green's function. The vectors $\underline{r}$ and $\underline{r'}$ are from the scattering origin to observation points and to source points on the scatterers, respectively. The Green's function can be expanded in terms of cylindrical

[1] Time factor of $e^{j\omega t}$ is suppressed

basis functions (in 2-D) as follows [11]:

$$g(k|\underline{r}-\underline{r'}|) = -j\frac{\pi}{2}\sum_n \psi_n(k\underline{r}_>)Rg\psi_n(k\underline{r}_<) \tag{3}$$

where $\psi_n(k\underline{r}) = H_n^{(2)}(kr)e^{-jn\phi}$ are the basis functions representing traveling waves and $Rg\psi_n(k\underline{r}) = J_n(kr)e^{-jn\phi}$ are the basis functions representing the standing waves. Here, Rg stands for "regular part of", $H_n^{(2)}(z)$ is the nth order Hankel function of second kind, $J_n(z)$ is the nth order Bessel function, and $\underline{r}_>$ ($\underline{r}_<$) means the larger (smaller) of $\underline{r}$ and $\underline{r'}$.

Based on the same decomposition, the scattered and incident fields can be expanded as [11]:

$$\psi^{sca}(\underline{r}) = \sum_n f_n\psi_n(\underline{r}) = \underline{\psi}^T\,\underline{f} \quad \text{if } |\underline{r}| > |\underline{r'}| \tag{4}$$

and

$$\psi^{inc}(\underline{r}) = \sum_n a_n Rg\psi_n(\underline{r}) = Rg\underline{\psi}^T\,\underline{a} \tag{5}$$

where $\underline{\psi}$ and $Rg\underline{\psi}$ are column vectors filled with $\psi_n(\underline{r})$ and $Rg\psi_n(\underline{r})$, respectively and ^{T} stands for transposition.

The T-matrix now is defined as [11,14]:

$$\underline{f} = \mathbf{T}\underline{a}. \tag{6}$$

The elements of $\mathbf{T}$ can be found by using (2), (3) and the boundary conditions. For a detailed analysis of the single object T-matrix method, the reader is referred to [14,15,11].

2.2 Recursive T-matrix Algorithm

The recursive T-matrix algorithm uses the basic principle of single scatterer T-matrix formulas in that for each object, the scattered fields from others are assumed a part of total incident field. This way for every scatterer a T-matrix can be assigned. The recursion starts with the T-matrices of individual scatterers, then one by one scatterers are incorporated into the equation and the T-matrices are updated until, for every scatterer, the final form of the T-matrix, including all multiple scattering effects, is obtained.

Formally, for L scatterers, the harmonic expansion of scattered field, similar to (4), can be written as [3]:

$$\psi^{sca}(\underline{r}) = \sum_{i=1}^{L} \underline{\psi}^T(\underline{r_i})\mathbf{T}_{i(L)}\boldsymbol{\beta}_{i,0}\underline{a} \tag{7}$$

where $\mathbf{T}_{i(L)}$ is the T-matrix for ith object in the presence of L scatterers and $\boldsymbol{\beta}_{i,0}$ is the translation matrix used to translate same type basis functions between scattering coordinate center (x_s, y_s) and ith object's local coordinate center (x_i, y_i), i.e. *standing* waves in ith local coordinate system to *standing* waves in 0th (scattering) coordinate system; or *traveling* waves in ith local coordinate system to *traveling* waves in 0th (scattering) coordinate system.[2] Fig. 1 pictorially shows the coordinate systems and how the translation matrices work. Expansion of the scattered field in (7) is valid if all observation points are outside the circle enclosing all scatterers. Following Chew's derivation, the recursive construction of $\mathbf{T}_{i(L)}$ can be written as [3, eq.10-11] :

$$\mathbf{T}_{n+1(n+1)}\boldsymbol{\beta}_{n+1,0} = \left[\mathbf{I} - \mathbf{T}_{n+1(1)}\sum_{i=1}^{n}\boldsymbol{\alpha}_{n+1,i}\mathbf{T}_{i(n)}\boldsymbol{\beta}_{i,0}\boldsymbol{\alpha}_{0,n+1}\right]^{-1}\mathbf{T}_{n+1(1)}\left[\boldsymbol{\beta}_{n+1,0} + \sum_{i=1}^{n}\boldsymbol{\alpha}_{n+1,i}\mathbf{T}_{i(n)}\boldsymbol{\beta}_{i,0}\right] \tag{8}$$

and

$$\mathbf{T}_{i(n+1)}\boldsymbol{\beta}_{i,0} = \mathbf{T}_{i(n)}\boldsymbol{\beta}_{i,0} + \mathbf{T}_{i(n)}\boldsymbol{\beta}_{i,0}\boldsymbol{\alpha}_{0,n+1}\mathbf{T}_{n+1(n+1)}\boldsymbol{\beta}_{n+1,0} \tag{9}$$

where $n = 1, 2, ..., L$, $i = 1, 2, ..., n$ and $\boldsymbol{\alpha}_{n,i}$ is the translation matrix used to change different basis functions between reference coordinate systems (Fig. 1), i.e. *standing* waves in nth local coordinate system to *traveling* waves in ith local coordinate system. The recursion starts with the individual T-matrices, $\mathbf{T}_{i(1)}$, of the scatterers, i.e. the T-matrix of the ith scatterer when there are no other scatterers in the medium.

Theoretically the matrices $\boldsymbol{\alpha}, \boldsymbol{\beta}, \mathbf{T}$ are of infinite dimension. T-matrix algorithms truncate these matrices with finite values N and M such that the residual error is below the machine precision

[2] The translation matrices $\boldsymbol{\beta}_{i,0}$ contain Bessel functions and complex exponentials. For details about these matrices see [1, 11].

or acceptable levels. Here N represents the number of harmonics used to expand the fields at the scattering origin and M represents the number of harmonics used to expand the fields in the objects' local coordinate systems. Thus, the T-matrix is of size $M \times M$, $\boldsymbol{\beta}_{i,0}$ is of size $M \times N$ and $\boldsymbol{\alpha}_{i,n+1}$ is of size $M \times M$. The parameters N and M are related to the distance of scatterers from the scattering origin and the radii of the scatterers, respectively. As the distances between scatterers and the scattering origin increase, N needs to be increased, and as the radii of scatterers increase, M needs to be increased [3].

3 A Modified Recursive T-Matrix Method

The work in this paper was motivated by the desire to obtain a fast, accurate forward modeling code for ground penetrating radar type geometries illustrated in Fig. 2. As discussed in Section 1 this application requires the computation of near field values of scattered field arising from mixtures of dielectric and metallic objects. To effectively handle these requirements, we propose a formulation of the recursive T-matrix algorithm based on the representation of the scattered field from each full object using high order expansions (i.e. large M) in the recursions in (8) and (9).

In principle, this approach supports the computation of scattered fields from arbitrary collections of dielectric and metallic objects. In fact, we demonstrate that this is true specifically for far-field calculations. Unfortunately, the use of higher order expansions results in an instability in a particular harmonic expansion formula upon which the original recursive T-matrix algorithm is based when near field computations are required. In the remainder of this section, we describe explicitly this difficulty and propose a modified recursion which by-passes this addition formula and results in a stable method for solving the problem of interest.

3.1 Determination of Scattering Origin

Unlike most radar applications, in a GPR measurement geometry the scattered field is generally observed in the near or intermediate field. Since the harmonic expansions upon which the recursive T-matrix algorithm is based have validity regions (see eqn.(4)), there are certain limitations as to where the scattering origin can be placed relative to the receiver array. In this section, we will briefly discuss how the scattering origin is determined, when the object locations and radii are given for the GPR-type configuration in Fig. 2. The triplet $(x_i, y_i; a_i)$ represents x and y coordinates and radius of the ith object relative to the global origin O_g and L is the number of objects buried under the receiver array.

Because of the requirements on the loci of observation points imposed by (4) for single objects and (7) for multiple objects, the scattering origin (x_s, y_s) relative to O_g must be selected such that there must be at least one circle, centered at (x_s, y_s), encircling all objects with no receivers inside it. The dashed circle in Fig. 2 depicts such a circle. Assuming a linear receiver array, the condition to choose the scattering coordinate system is:

$$R_c < |y_s| \tag{10}$$

where

$$R_c = \max_{i \in \{1,2,\ldots,L\}} \left\{ \sqrt{(x_s - x_i)^2 + (y_s - y_i)^2} + a_i \right\}. \tag{11}$$

This condition must be met by individual objects as well as by all objects collectively. Therefore, we can rewrite the condition in (10) and (11) as the intersection of regions as follows:

$$(x_s, y_s) \in \left\{ (x, y) | \bigcap_{i=1}^{L} \sqrt{(x - x_i)^2 + (y - y_i)^2} < |y| - a_i \right\}. \tag{12}$$

In fact, each term under the intersection sign in (12) defines the region under an upside-down parabola. Fig. 3 depicts the parabolic regions for three objects. Placement of objects in this figure is very typical of a mine detection problem. In this geometry, any point inside the shaded

area, representing the intersection of all three parabolic regions, can be selected as the scattering origin. Ideally, we can place the scattering origin at $y_s \approx -\infty$. This choice of (x_s, y_s) will always satisfy the condition in (10). However, the order of harmonics used in the T-matrix algorithm is proportional to the distance between scattering origin and object centers [3], i.e. $N \propto kr_i$ where N is the harmonic used for translations to and from the scattering origin, k is the wave number and $i = 1, 2, ..., L$. Therefore, the optimum scattering origin should be within this shaded area and as close as possible to the objects in order to minimize the harmonics used for translations. As we show in Section 3.2, with this choice of (x_s, y_s), the distances between object centers and the scattering origin can be very close, which causes convergence problems in the addition formulas of T-matrix algorithm. In Section 3.3, we describe a modification in the recursive T-matrix algorithm that lets us use the algorithm with optimum choice of scattering origin.

3.2 Problems With Higher Order Harmonic Expansions

The convergence problems alluded to earlier can be traced to the fact that equation (8) uses the identity

$$\boldsymbol{\alpha}_{p,q} = \boldsymbol{\beta}_{p,0}\boldsymbol{\alpha}_{0,q} \qquad \text{if } |\underline{r}_q| \geq |\underline{r}_p| \tag{13}$$

which in turn requires the ordering of the objects such that $|\underline{r}_1| \leq |\underline{r}_2| \leq ... \leq |\underline{r}_L|$. By using definitions of $\boldsymbol{\alpha}_{p,q}$, $\boldsymbol{\beta}_{p,0}$ and $\boldsymbol{\alpha}_{0,q}$ [1,11], we can write the (m, m')th entry, $[\boldsymbol{\alpha}_{p,q}]_{m,m'}$, as:

$$H^{(2)}_{m-m'}(k|\underline{r}_{pq}|)e^{-j(m-m')\phi_{pq}} = \lim_{N\to\infty} \sum_{n=-N}^{N} J_{m-n}(k|\underline{r}_p|)e^{-j(m-n)(\phi_p+\pi)} H^{(2)}_{n-m'}(k|\underline{r}_q|)e^{-j(n-m')\phi_q} \tag{14}$$

where $\underline{r}_{pq} = |\underline{r}_{pq}|e^{-j\phi_{pq}} = \underline{r}_q - \underline{r}_p$ and $\underline{r}_i = |\underline{r}_i|e^{-j\phi_i}$, $i = p, q$. This truncated sum does not converge if $\underline{r}_q = \underline{r}_p + \underline{\delta}$ where $|\underline{\delta}|$ is small as compared to $|\underline{r}_p|$ and $|\underline{r}_q|$, and if $m - m'$ is a large number ($-M \leq m \leq M$ and $-M \leq m' \leq M$.) Fig. 4 shows the convergence of the series in (14) for the corner entries of (13) for $M = 5$, i.e. $\max\{m - m' = 10\}$. Here we have three curves, showing the

convergence for $\underline{\delta} = 0.1\underline{r}_p$, $\underline{\delta} = 0.25\underline{r}_p$ and $\underline{\delta} = 0.5\underline{r}_p$, $M \geq 5$ and $\underline{\delta} < 0.1\underline{r}_p$ are typical parameter choices for the problems of interest in this paper. It is clear from this figure that as the magnitudes of two vectors get closer, the convergence rate slows. Chew et.al. [4] suggested a windowed addition theorem (which is originally developed for H_z polarized scattering) to overcome this problem, but the implementation of this method introduces two new variables to choose in order to set the width and shape of the window. In addition, the implementation of windowed summation introduces errors in the sum for vectors for which the convergence is not a problem.

It should be noted that not all valid scattering origins for a given problem give rise to this convergence problem. Indeed, trial an error will quickly demonstrate that, for a given collection of scatterers, there exist scattering origins where the original T-matrix recursions work just fine. These points are typically far from the scatterers thereby requiring large N in the recursions and moreover there does not appear to be an easy means of *a priori* determining whether a chosen origin will or will not give rise to a covergence difficulty. Thus, in the following sections, we introduce a modified recursion which bypasses the convergence issue for all valid scattering origins thereby allowing us to use the closest valid origin (i.e. smallest N) to solve the problem.

3.3 Modified Recursive T-Matrix Algorithm

The recursion in (8) and (9) takes place over the quantities $\mathbf{T}_{i(n)}\boldsymbol{\beta}_{i,0}$, and we have determined that the convergence problem stems from (13). Therefore, to eliminate the need to use this identity, we go one step back in the derivation of recursion formulas, and write (8) as [3, eq.7-8]:

$$\mathbf{T}_{n+1(n+1)}\boldsymbol{\beta}_{n+1,0} = \left[\mathbf{I} - \mathbf{T}_{n+1(1)}\sum_{i=1}^{n}\boldsymbol{\alpha}_{n+1,i}\mathbf{T}_{i(n)}\boldsymbol{\alpha}_{i,n+1}\right]^{-1}\mathbf{T}_{n+1(1)}\left[\boldsymbol{\beta}_{n+1,0} + \sum_{i=1}^{n}\boldsymbol{\alpha}_{n+1,i}\mathbf{T}_{i(n)}\boldsymbol{\beta}_{i,0}\right] \tag{15}$$

and (9) as:

$$\mathbf{T}_{i(n+1)}\boldsymbol{\beta}_{i,0} = \mathbf{T}_{i(n)}\left[\boldsymbol{\beta}_{i,0} + \boldsymbol{\alpha}_{i,n+1}\mathbf{T}_{n+1(n+1)}\boldsymbol{\beta}_{n+1,0}\right] \tag{16}$$

without using (13). Since (13) is not used in (15) and (16) we can base a new recursion on these two equations and the identity:

$$\boldsymbol{\beta}_{i,0}\boldsymbol{\beta}_{0,i} = \mathbf{I} \tag{17}$$

where $\boldsymbol{\beta}_{i,0}$ is $M \times N$, $\boldsymbol{\beta}_{0,i}$ is $N \times M$, and (17) holds as long as $N > M$ which is always true as long as objects are not overlapping. By using (15), (16) and (17) the modified recursion equations can be written as:

$$\mathbf{T}_{n+1(n+1)}\boldsymbol{\beta}_{n+1,0} = \left[\mathbf{I} - \mathbf{T}_{n+1(1)}\sum_{i=1}^{n}\boldsymbol{\alpha}_{n+1,i}\mathbf{T}_{i(n)}\boldsymbol{\beta}_{i,0}\boldsymbol{\beta}_{0,i}\boldsymbol{\alpha}_{i,n+1}\right]^{-1}\mathbf{T}_{n+1(1)}\left[\boldsymbol{\beta}_{n+1,0} + \sum_{i=1}^{n}\boldsymbol{\alpha}_{n+1,i}\mathbf{T}_{i(n)}\boldsymbol{\beta}_{i,0}\right] \tag{18}$$

and

$$\mathbf{T}_{i(n+1)}\boldsymbol{\beta}_{i,0} = \mathbf{T}_{i(n)}\boldsymbol{\beta}_{i,0} + \mathbf{T}_{i(n)}\boldsymbol{\beta}_{i,0}\boldsymbol{\beta}_{0,i}\boldsymbol{\alpha}_{i,n+1}\mathbf{T}_{n+1(n+1)}\boldsymbol{\beta}_{n+1,0}. \tag{19}$$

Note that the recursion is still over the same block, $\mathbf{T}_{i(n)}\boldsymbol{\beta}_{i,0}$, but since (13) is eliminated these new recursion equations do not suffer from convergence problems.

As reported in [3] the original recursive T-matrix algorithm has a complexity of $O(M^2N)$ per recursion. It is easily shown that the modified algorithm also has a complexity of $O(M^2N)$ per recursion with a slightly larger constant in front of M^2N resulting from extra multiplications to obtain $\mathbf{T}_{i(n)}$ from $\mathbf{T}_{i(n)}\boldsymbol{\beta}_{i,0}$. To calculate the scattered field from L objects, $L(L-1)/2$ recursions are required. Therefore, the overall complexity of both the recursive and modified recursive algorithm is $O(L^2M^2N)$.

4 Discussion And Examples

In this section, we first verify our new scattering algorithm against published results and then provide a collection of examples that are particularly relevant for near field, GPR-type applications. As most previously published results for mixed scatterer problems involve far field computations, in verifying our approach we also demonstrate its ability to handle far zone calculations. Where

appropriate, we compare the computational complexity of our higher order, modified recursive algorithm (HO-MRA) against two alternate T-matrix approaches. First, we implement the lower order, original recursive algorithm (LO-ORA) of [3] for near and far field, dielectric-only problems. For far zone problems with mixtures of dielectric and metallic scatterers, we consider high order (i.e. large M) forms of the original recursions (labeled HO-ORA here) (8) and (9), where, because of the far field assumption, the instability problem is not an issue.

Before we proceed, we define the terms used in this section. The echo width, i.e. scattering cross-section per unit length, and normalized echo width are defined as [10]:

$$\sigma(\phi) = \lim_{r\to\infty} 2\pi r \left| \frac{\psi^{sca}(\underline{r})}{\psi^{inc}(\underline{r})} \right|^2, \tag{20}$$

and

$$\sigma_n(\phi) = \sqrt{\frac{\sigma(\phi)}{\lambda}} \tag{21}$$

where λ is the wavelength in the medium of propagation. The normalized scattering field pattern is defined as:

$$F(\phi) = 10\log_{10}\left\{ \lim_{r\to\infty} 2\pi r \frac{|\psi^{sca}(\underline{r})|^2}{\max\{|\psi^{sca}(\underline{r})|^2\}} \right\}. \tag{22}$$

In order to ensure that the modified algorithm can indeed find the true scattered fields, we verified our calculations against published scattered field patterns. We first calculated the scattered field due to two dielectric cylinders placed in free space, each with relative dielectric constant of 2.6, and radius of 0.5λ. The distance between the cylinders is 3λ (Fig. 5(a).) An E_z polarized planewave is incident from 0°. Fig. 5(b) shows the echo width calculated using the HO-MRA of this paper (solid line), the LO-ORA of [3] (dashed line) and results in [10] (circles). Fig. 6(b) shows a similar comparison for a mixed object case depicted in Fig. 6(a), i.e. one cylinder is metallic and the other is lossy dielectric with $\epsilon_r = 4 - j5$. For this case, we did not include the echo width calculated using the original recursive algorithm, since the method in [3] is limited to dielectric

objects. As in previous examples, the echo width obtained using the modified algorithm and that reported in [10] are very close.

Next, we compared the scattering patterns for two metallic cylinders. In this case both cylinders have a radius of 1.1λ ($ka = 7$) and separated by a distance of 2.6λ ($kd = 16$.) Fig. 7(a) shows the scattering geometry for this example and (b) shows the scattered field patterns of both our solution (solid line) and the one given in [5] (circles.) As seen from these figures, the scattering pattern obtained using the modified algorithm and that given in [5] are very close.

Now, we present scattering examples that are especially useful in GPR applications. All objects are assumed to be buried in a homogeneous, lossy background ($\epsilon_b = 6\epsilon_0$, $\sigma_b = 5 \times 10^{-2} S/m$; typical properties of 5% moist San Antonio clay loam or 10% moist Puerto Rico clay loam [7]); the operating frequency is $1GHz$ and a planewave is incident from 90°, see Fig. 8(a). We first find the scattered field from 3 dielectric mine-like objects with diameters $7.5cm$ as shown in Fig. 8(a). All objects have a relative permittivity of 2.5. The scattering origin has to be placed far away from the receiver array ($x_s = 0.5m$, $y_s = -1.25m$), because the objects are close to the receivers, which in turn requires a large value, 120, for N. For this case, we calculated the scattered field using both the LO-ORA and HO-MRA defined in Section 2.2 and Section 3.3, respectively. Fig. 8(b) shows the scattered fields observed along the receiver array using the HO-MRA (solid line) and the LO-ORA (circles). It is clear from this figure that both approaches yield very similar fields but the computational complexity (flop count) of our method is 18.94×10^6 flops while that of the tesselated scheme is 1671×10^6 flops.

The second GPR example depicts a mixed mine-like object case since the objects at the sides are metallic and the object at the center is dielectric with a relative dielectric constant of 2.5, Fig. 9(a). The mine-like geometry is unchanged and the scattering origin is still at ($x_s = 0.5m$, $y_s = -1.25m$).

As a result $N = 120$, and since the object radii are relatively small $M = 12$. The scattered field observed along the receiver array for mixed mine-like object case is shown in Fig.9(b). The last example demonstrates the calculation of scattered field from buried waste drums. For this case we have 2 metallic drums of radius $0.3m$ buried in the same lossy background before, as shown in Fig. 10(a). The scattering origin is placed at ($x_s = 1m$, $y_s = -1.37m$) to minimize the harmonics used in the expansions ($M = 25$, $N = 110$). For drum case M is quite large since the radii of the objects are considerably large. Fig. 10(b) shows the scattered field observed along the receiver array placed directly above the cylinders.

Having verified the scattering field patterns of new recursion with the ones in the literature and presented the GPR examples, we compared the complexities of the HO-MRA, LO-ORA, and HO-ORA. To ensure a fair comparison, whenever a tessellation is required, we set the density of sub-scatterers to be close to that used in [3]. Performance of the each approach is measured by the floating point operations (flops) required to calculate the scattered field. Table 1 shows the flop count of all three recursive T-matrix algorithms that can be used to find the scattered fields from multiple, spatially separated cylinders. Table 2 shows the number of scatterers L, harmonics M, N and the location of the scattering origin (x_s, y_s) used in these examples.

The first three rows of Tables 1 and 2 correspond to examplesfrom the two dimensional scattering literature. For these cases, all observation points are in the far field so that the convergence problem alluded to earlier is not an issue. As a result, with dielectric objects HO-MRA, LO-ORA and HO-ORA can be used to calculate the scattered field. LO-ORA is used only with dielectric objects [3] and as seen from Table 1 its computational complexity is quite large as compared to HO-MRA and HO-ORA. The reason behind this large complexity is that numerous sub-scatterers are required for each cylinder. The computational complexity of HO-ORA is at most 15% less than that of

HO-MRA since the latter needs extra multiplications to obtain $\mathbf{T}_{i(n)}$ from $\mathbf{T}_{i(n)}\boldsymbol{\beta}_{i,0}$.

The last three rows of Table 1 show the flops needed to find the scattered field for GPR-specific examples and Table 2 shows the number of scatterers, harmonics and the locus of the scattering origin used in these examples. The geometries of GPR cases of interest are depicted in Figures 8(a), 9(a) and 10(a). Unlike previous examples, GPR problems require measuring the scattered field in the near field, which restricts the regions where the scattering origin can be placed. As we have shown in Section 3, the choice of optimum scattering origin results in convergence problems in HO-ORA, making it inaccessible for GPR geometries. In addition LO-ORA is not used with metallic objects leaving only HO-MRA for all GPR geometries and all material types. Even when LO-ORA is used for dielectric-only objects, one has to spend approx. 88 times more flops than it is needed for HO-MRA (Table 1).

5 Conclusions

In this paper, we present a new recursive T-matrix algorithm specifically designed for the efficient solution of near field scattering problems involving heterogeneous collections of metallic and dielectric objects. We have verified this algorithm against previously published results thereby demonstrating its utility for far field computations and indicated its use for GPR-type scattering problems. For near and far-field dielectric scattering problems, this algorithm is significantly more efficient than the sub-scatterer method in [3]. For far-field computations, the technique in this paper is slightly more costly than the use of higher order expansions in the original recursive formulae.

The work in this paper suggests a variety of additional research directions. First, we are quite interested in extending the modified recursive algorithm into three dimensions while simultaneously considering scattering problems involving irregularly shaped objects where the T-matrices would be

computed using the method of moments as in [4]. Such work would allow for the easy examination as to how object shape and orientation impacts the scattered fields and ultimately, the ability to detect and localize objects. In terms of the GPR application which originally motivated this effort, we are looking to T-matrix type methods which might allow for some level of modeling the air-earth interface relevant in these scenarios without destroying the computational efficiency of the scattering model. Finally, applying the near field computational abilities of this approach to other application areas would be quite interesting.

References

[1] W.C. Chew. *Waves and Fields in Inhomogeneous Media.* Van Nostrand Reinhold, 1990.

[2] Weng Cho Chew, James A. Friedrich, and Robert Geiger. A multiple scattering solution for effective permittivity of a sphere mixture. *IEEE Trans. Geoscience and Remote Sensing*, 28(2):207–214, March 1990.

[3] Y.M. Wang W.C. Chew. An efficient algorithm for solution of a scattering problem. *Microwave and Optical Technology Letters*, 3(3):102–106, March 1990.

[4] W.C. Chew Y.M. Wang L. Gürel. Recursive algorithm for wave-scattering solutions using windowed addition theorem. *Journal of Electromagnetic Waves and Applications*, 6(11):1537–1560, 1992.

[5] A.Z. Elsherbeni M. Hamid. Scattering by parallel conducting circular cylinders. *IEEE Trans. on Antennas and Propagation*, 35(3):355–358, March 1987.

[6] R.F. Harrington. *Field Computation by Moment Methods.* IEEE Press, (Originally published: Malabar, Fla. :R.E. Krieger, 1968), 1993.

[7] J.E. Hipp. Soil electromagnetic parameters as functions of frequency, soil density, and soil moisture. *Proceedings of the IEEE*, 62(1):98–103, January 1974.

[8] W.C. Chew L. Gürel Y.M. Wang G. Otto R.L. Wagner Q.H. Liu. A generalized recursive algorithm for wave-scattering solutions in two dimensions. *IEEE Trans. on Microwave Theory and Techniques*, 40(4):716–722, April 1992.

[9] V. Rokhlin. Rapid solution of integral equations of scattering theory in two dimensions. *Journal of Computational Physics*, 86(2):414–439, 1990.

[10] M. Ouda M. Hussein A. Sebak. Multiple scattering by dielectric cylinders using a multi-filament current model. *Journal of Electromagnetic Waves and Applications*, 7(2):215–234, 1993.

[11] B. Peterson S. Ström. Matrix formulation of acoustic scattering from an arbitrary number of scatterers. *J. Acoust. Soc. Am.*, 56(3):771–780, September 1974.

[12] N. Engheta W.D. Murphy V. Rokhlin M.S. Vassiliou. The fast multipole method (FMM) for electromagnetic scattering problems. *IEEE Trans. on Antennas and Propagation*, 40(6):634–641, June 1992.

[13] W.C. Chew Y.M. Wang. A fast algorithm for solution of a scattering problem using a recursive aggregate τ matrix method. *Microwave and Optical Technology Letters*, 3(5):164–169, May 1990.

[14] P.C. Waterman. New formulation of acoustic scattering. *J. Acoust. Soc.*, 45(6):1417–1429, 1969.

[15] P.C. Waterman. Symmetry, unitarity and geometry in electromagnetic scattering. *Physical Review D*, 3(4):825–839, February 1971.

	HO-MRA	LO-ORA	HO-ORA
Fig. 5	0.6	1150	0.55
Fig. 6	1.9	n/a	1.76
Fig. 7	8.84	n/a	7.73
Fig. 8	18.94	1671	c/p
Fig. 9	18.95	n/a	c/p
Fig. 10	29.5	n/a	c/p

Table 1: Complexity Comparison for Recursive Algorithms. All numbers in FLOPS/10^6, n/a means not applicable and c/p means convergence problems

	HO-MRA	LO-ORA	HO-ORA
Fig. 5	L=2,M=7,N=23 (x_s, y_s)=(0,0)	L=398,M=1,N=23 (x_s, y_s)=(0,0)	L=2,M=7,N=23 (x_s, y_s)=(0.5λ ,0.5λ)
Fig. 6	L=2,M=10,N=40 (x_s, y_s)=(0,0)	n/a	L=2,M=10,N=40 (x_s, y_s)=(0.5λ ,0.5λ)
Fig. 7	L=2,M=20,N=40 (x_s, y_s)=(0,0)	n/a	L=2,M=20,N=40 (x_s, y_s)=(λ ,λ)
Fig. 8	L=3,M=12,N=120 (x_s, y_s)=(0.5,-1.25)	L=93,M=3,N=120 (x_s, y_s)=(0.5,-1.25)	c/p
Fig. 9	L=3,M=12,N=120 (x_s, y_s)=(0.5,-1.25)	n/a	c/p
Fig. 10	L=2,M=25,N=110 (x_s, y_s)=(1,-1.37)	n/a	c/p

Table 2: Parameter list for Table 1

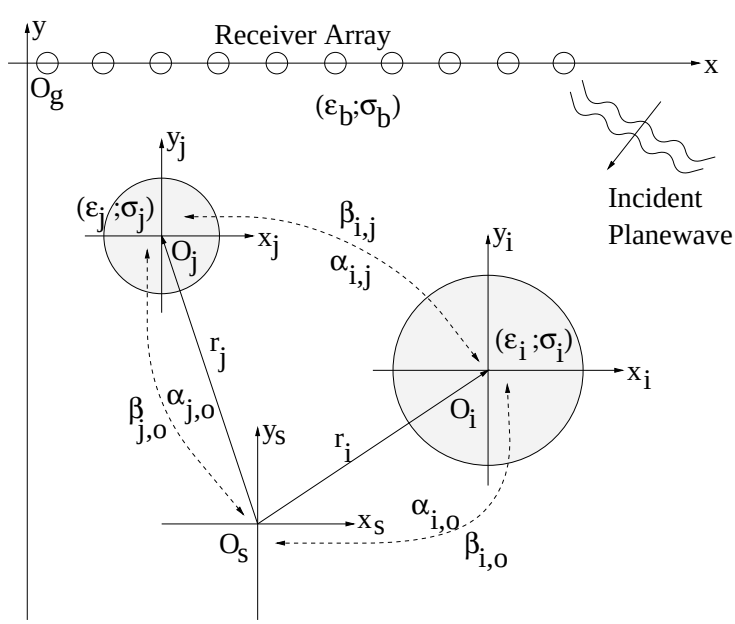

Figure 1: GPR geometry and translation matrices

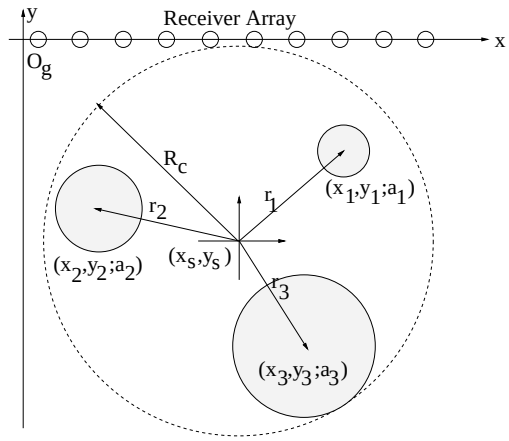

Figure 2: Scattering origin relative to the scatterers, the global origin O_g and the receivers

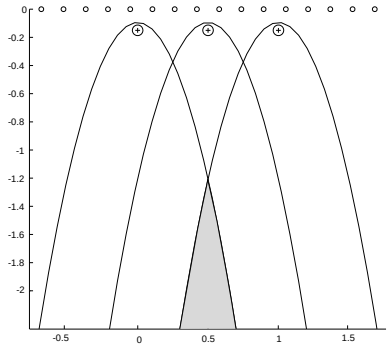

Figure 3: Scattering Origin Regions

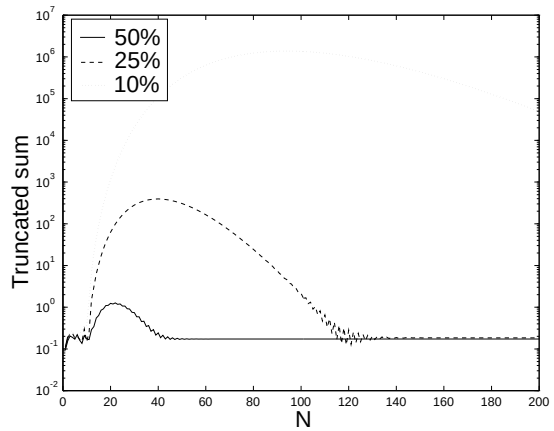

Figure 4: Convergence pattern of the truncated sum in (14) for M=5. Curves show the convergence for $\underline{\delta} = 0.1\underline{r}_p$, $\underline{\delta} = 0.25\underline{r}_p$ and $\underline{\delta} = 0.5\underline{r}_p$.

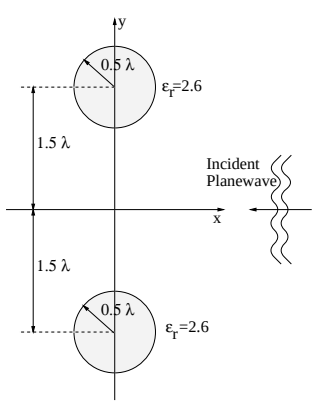

(a) Scattering geometry

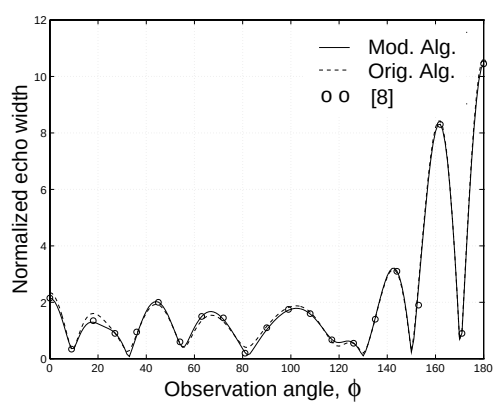

(b) Normalized echo width for geometry of (a)

Figure 5: Comparison of echo width with [10] for two equal dielectric cylinders

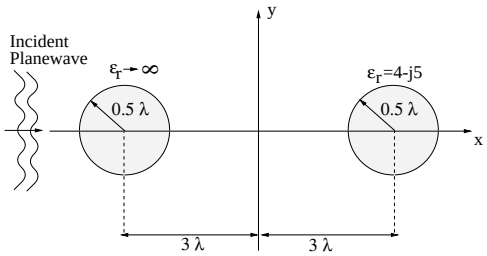

(a) Scattering geometry

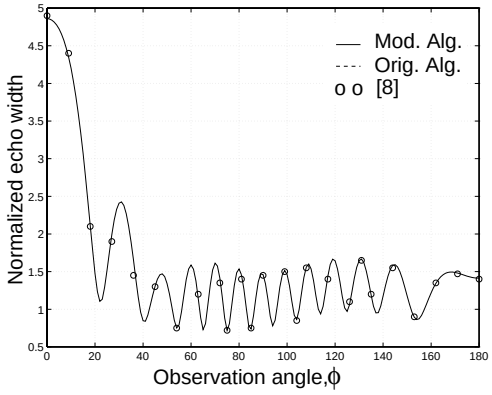

(b) Normalized echo width for geometry of (a)

Figure 6: Comparison of echo width with [10] for two cylinders, one lossy dielectric and one metallic

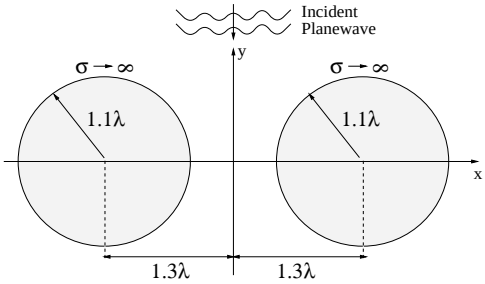

(a) Scattering geometry

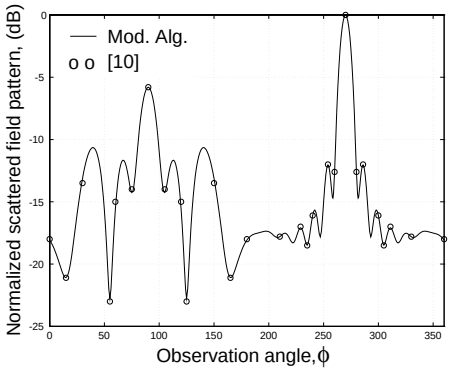

(b) Scattered field pattern for geometry of (a)

Figure 7: Comparison of scattered field pattern with [5] for two metallic cylinders

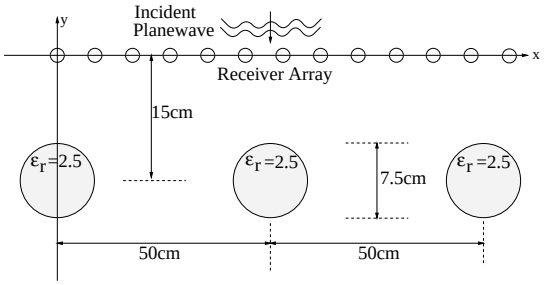

(a) GPR-type mine detection geometry

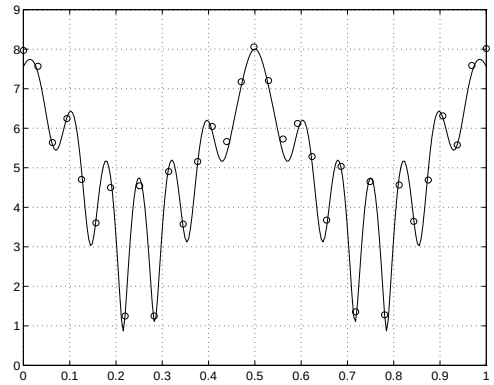

(b) Scattered field observed along the receivers for geometry of (a)

Figure 8: Implementation of T-matrix method to calculate the scattered field from 3 dielectric mine-like objects

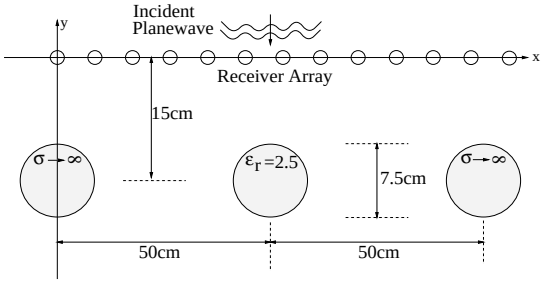

(a) GPR-type mine detection geometry

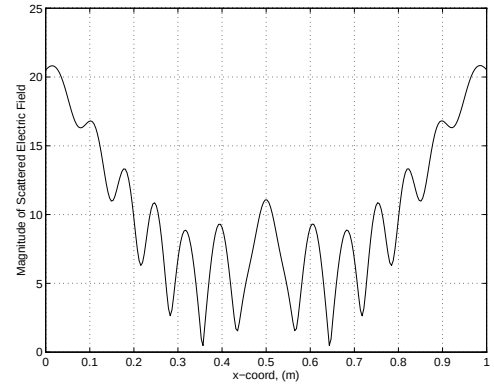

(b) Scattered field observed along the receivers for geometry of (a)

Figure 9: Implementation of T-matrix method to calculate the scattered field from 2 metallic and a dielectric mine-like objects

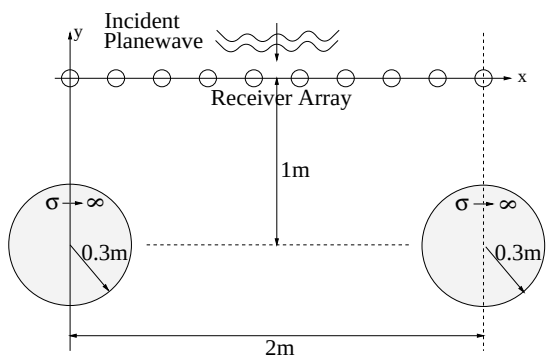

(a) GPR-type drum detection and localization geometry

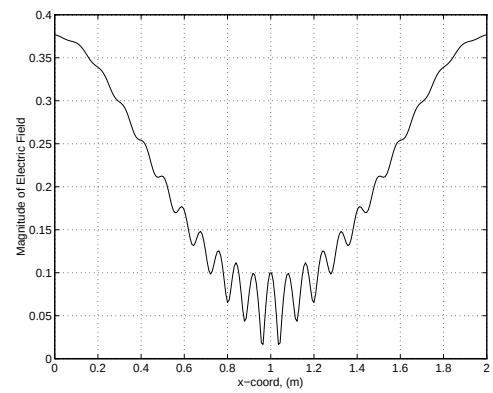

(b) Scattered field observed along the receivers for geometry of (a)

Figure 10: Implementation of T-matrix method to calculate the scattered field from drum-like objects